Appendix A

Modified GRIMECH 3.0 Reaction Mechanism

The following is a listing of the file gri3_r2.mec which is the mechanism used in both Bunsen type burner and Honeycomb burner modeling calculations. Only the reactions are shown here. Other elements of the reaction mechanism file such as the elements and species contained are omitted. Also, for brevity, the collision efficiencies of third–body reactions are omitted. Third–body efficiencies were not modified in the revisions to GRIMECH 3.0 (Smith et al., 1999) and so may be obtained from the cited web–page. The reaction mechanism shows which of the reactions are considered reversible. An equal sign surrounded by opposing arrows means that the reaction in question is reversible. If the equal sign is merely followed by an arrow, the reaction in question is not reversible. All the reactions involving chemiluminescent species are irreversible, since equilibrium coefficients for these reactions are difficult to define. It is noteworthy however, that especially at higher pressures, the thermal excitation of molecules by collision may become significant. Currently, however, the collisions are considered only to extract energy from the excited molecule. In the present model, collisions between two unexcited molecules do not cause the excitation of one of them, hence not allowing thermal excitation.

(Reaction listing begins on the next page)

Reaction Form	Reaction Constant	Temperature Exponent	Activation Energy (cal/mole)
2O+M<=>O2+M	1.200E+17	-1.000	.00
O+H+M<=>OH+M	5.000E+17	-1.000	.00
O+H2<=>H+OH	3.870E+04	2.700	6260.00
O+HO2<=>OH+O2	2.000E+13	.000	.00
O+H2O2<=>OH+HO2	9.630E+06	2.000	4000.00
O+CH<=>H+CO	5.700E+13	.000	.00
O+CH2<=>H+HCO	8.000E+13	.000	.00
O+CH2(S)<=>H2+CO	1.500E+13	.000	.00
O+CH2(S)<=>H+HCO	1.500E+13	.000	.00
O+CH3<=>H+CH2O	5.060E+13	.000	.00
O+CH4<=>OH+CH3	1.020E+09	1.500	8600.00
O+CO(+M)<=>CO2(+M)	1.800E+10	.000	2385.00
O+HCO<=>OH+CO	3.000E+13	.000	.00
O+HCO<=>H+CO2	3.000E+13	.000	.00
O+CH2O<=>OH+HCO	3.900E+13	.000	3540.00
O+CH2OH<=>OH+CH2O	1.000E+13	.000	.00
O+CH3O<=>OH+CH2O	1.000E+13	.000	.00
O+CH3OH<=>OH+CH2OH	3.880E+05	2.500	3100.00
O+CH3OH<=>OH+CH3O	1.300E+05	2.500	5000.00
O+C2H<=>CH+CO	2.500E+13	.000	.00

Reaction Form	Reaction Constant	Temperature Exponent	Activation Energy (cal/mole)
O+C2H2<=>H+HCCO	1.350E+07	2.000	1900.00
O+C2H2<=>OH+C2H	1.431E+05	2.000	1900.00
O+C2H2<=>CO+CH2	6.940E+06	2.000	1900.00
O+C2H3<=>H+CH2CO	3.000E+13	.000	.00
O+C2H4<=>CH3+HCO	1.250E+07	1.830	220.00
O+C2H5<=>CH3+CH2O	2.240E+13	.000	.00
O+C2H6<=>OH+C2H5	8.980E+07	1.920	5690.00
O+HCCO<=>H+2CO	1.000E+14	.000	.00
O+CH2CO<=>OH+HCCO	1.000E+13	.000	8000.00
O+CH2CO<=>CH2+CO2	1.750E+12	.000	1350.00
O2+CO<=>O+CO2	2.500E+12	.000	47800.00
O2+CH2O<=>HO2+HCO	1.000E+14	.000	40000.00
H+O2+M<=>HO2+M	2.800E+18	-.860	.00
H+2O2<=>HO2+O2	2.080E+19	-1.240	.00
H+O2+H2O<=>HO2+H2O	11.26E+18	-.760	.00
H+O2+N2<=>HO2+N2	2.600E+19	-1.240	.00
H+O2<=>O+OH	2.650E+16	-.6707	17041.00
2H+M<=>H2+M	1.000E+18	-1.000	.00
2H+H2<=>2H2	9.000E+16	-.600	.00
2H+H2O<=>H2+H2O	6.000E+19	-1.250	.00
2H+CO2<=>H2+CO2	5.500E+20	-2.000	.00

Reaction Form	Reaction Constant	Temperature Exponent	Activation Energy (cal/mole)
H+OH+M<=>H2O+M	2.200E+22	-2.000	.00
H+HO2<=>O+H2O	3.970E+12	.000	671.00
H+HO2<=>O2+H2	4.480E+13	.000	1068.00
H+HO2<=>2OH	0.840E+14	.000	635.00
H+H2O2<=>HO2+H2	1.210E+07	2.000	5200.00
H+H2O2<=>OH+H2O	1.000E+13	.000	3600.00
H+CH2(+M)<=>CH3(+M)	6.000E+14	.000	.00
H+CH2(S)<=>CH+H2	3.000E+13	.000	.00
H+CH3(+M)<=>CH4(+M)	13.90E+15	-.534	536.00
H+CH4<=>CH3+H2	6.600E+08	1.620	10840.00
H+HCO(+M)<=>CH2O(+M)	1.090E+12	.480	-260.00
H+HCO<=>H2+CO	7.340E+13	.000	.00
H+CH2O(+M)<=>CH2OH(+M)	5.400E+11	.454	3600.00
H+CH2O(+M)<=>CH3O(+M)	5.400E+11	.454	2600.00
H+CH2O<=>HCO+H2	5.740E+07	1.900	2742.00
H+CH2OH(+M)<=>CH3OH(+M)	1.055E+12	.500	86.00
H+CH2OH<=>H2+CH2O	2.000E+13	.000	.00
H+CH2OH<=>OH+CH3	1.650E+11	.650	-284.00
H+CH2OH<=>CH2(S)+H2O	3.280E+13	-.090	610.00
H+CH3O(+M)<=>CH3OH(+M)	2.430E+12	.515	50.00

Reaction Form	Reaction Constant	Temperature Exponent	Activation Energy (cal/mole)
H+CH3O<=>H+CH2OH	4.150E+07	1.630	1924.00
H+CH3O<=>H2+CH2O	2.000E+13	.000	.00
H+CH3O<=>OH+CH3	1.500E+12	.500	-110.00
H+CH3O<=>CH2(S)+H2O	2.620E+14	-.230	1070.00
H+CH3OH<=>CH2OH+H2	1.700E+07	2.100	4870.00
H+CH3OH<=>CH3O+H2	4.200E+06	2.100	4870.00
H+C2H(+M)<=>C2H2(+M)	2.500E+17	-1.000	.00
H+C2H2(+M)<=>C2H3(+M)	5.600E+12	.000	2400.00
H+C2H3(+M)<=>C2H4(+M)	6.080E+12	.270	280.00
H+C2H3<=>H2+C2H2	3.000E+13	.000	.00
H+C2H4(+M)<=>C2H5(+M)	0.540E+12	.454	1820.00
H+C2H4<=>C2H3+H2	1.325E+06	2.530	12240.00
H+C2H5(+M)<=>C2H6(+M)	5.210E+17	-.990	1580.00
H+C2H5<=>H2+C2H4	2.000E+12	.000	.00
H+C2H6<=>C2H5+H2	1.150E+08	1.900	7530.00
H+HCCO<=>CH2(S)+CO	1.000E+14	.000	.00
H+CH2CO<=>HCCO+H2	5.000E+13	.000	8000.00
H+CH2CO<=>CH3+CO	1.130E+13	.000	3428.00
H+HCCOH<=>H+CH2CO	1.000E+13	.000	.00
H2+CO(+M)<=>CH2O(+M)	4.300E+07	1.500	79600.00

Reaction Form	Reaction Constant	Temperature Exponent	Activation Energy (cal/mole)
OH+H2<=>H+H2O	2.160E+08	1.510	3430.00
2OH(+M)<=>H2O2(+M)	7.400E+13	-.370	.00
2OH<=>O+H2O	3.570E+04	2.400	-2110.00
OH+HO2<=>O2+H2O	1.450E+13	.000	-500.00
DUPLICATE			
OH+H2O2<=>HO2+H2O	2.000E+12	.000	427.00
DUPLICATE			
OH+H2O2<=>HO2+H2O	1.700E+18	.000	29410.00
DUPLICATE			
OH+CH<=>H+HCO	3.000E+13	.000	.00
OH+CH2<=>H+CH2O	2.000E+13	.000	.00
OH+CH2<=>CH+H2O	1.130E+07	2.000	3000.00
OH+CH2(S)<=>H+CH2O	3.000E+13	.000	.00
OH+CH3(+M)<=>CH3OH(+M)	2.790E+18	-1.430	1330.00
OH+CH3<=>CH2+H2O	5.600E+07	1.600	5420.00
OH+CH3<=>CH2(S)+H2O	6.440E+17	-1.340	1417.00
OH+CH4<=>CH3+H2O	1.000E+08	1.600	3120.00
OH+CO<=>H+CO2	4.760E+07	1.228	70.00
OH+HCO<=>H2O+CO	5.000E+13	.000	.00
OH+CH2O<=>HCO+H2O	3.430E+09	1.180	-447.00
OH+CH2OH<=>H2O+CH2O	5.000E+12	.000	.00
OH+CH3O<=>H2O+CH2O	5.000E+12	.000	.00

Reaction Form	Reaction Constant	Temperature Exponent	Activation Energy (cal/mole)
OH+CH3OH<=>CH2OH+H2O	1.440E+06	2.000	-840.00
OH+CH3OH<=>CH3O+H2O	6.300E+06	2.000	1500.00
OH+C2H<=>H+HCCO	2.000E+13	.000	.00
OH+C2H2<=>H+CH2CO	5.418E-01	3.180	-8754.00
OH+C2H2<=>H+HCCOH	1.831E+11	0.300	6500.00
OH+C2H2<=>C2H+H2O	1.225E+13	0.000	7000.00
OH+C2H2<=>CH3+CO	1.755E+02	2.000	-9000.00
OH+C2H3<=>H2O+C2H2	5.000E+12	.000	.00
OH+C2H4<=>C2H3+H2O	3.600E+06	2.000	2500.00
OH+C2H6<=>C2H5+H2O	3.540E+06	2.120	870.00
OH+CH2CO<=>HCCO+H2O	7.500E+12	.000	2000.00
2HO2<=>O2+H2O2	1.300E+11	.000	-1630.00
DUPLICATE			
2HO2<=>O2+H2O2	4.200E+14	.000	12000.00
DUPLICATE			
HO2+CH2<=>OH+CH2O	2.000E+13	.000	.00
HO2+CH3<=>O2+CH4	1.000E+12	.000	.00
HO2+CH3<=>OH+CH3O	3.780E+13	.000	.00
HO2+CO<=>OH+CO2	1.500E+14	.000	23600.00
HO2+CH2O<=>HCO+H2O2	5.600E+06	2.000	12000.00
CH+O2<=>O+HCO	6.710E+13	.000	.00
CH+H2<=>H+CH2	1.080E+14	.000	3110.00

Reaction Form	Reaction Constant	Temperature Exponent	Activation Energy (cal/mole)
CH+H2O<=>H+CH2O	5.710E+12	.000	-755.00
CH+CH2<=>H+C2H2	4.000E+13	.000	.00
CH+CH3<=>H+C2H3	3.000E+13	.000	.00
CH+CH4<=>H+C2H4	6.000E+13	.000	.00
CH+CO(+M)<=>HCCO(+M)	5.000E+13	.000	.00
CH+CO2<=>HCO+CO	1.900E+14	.000	15792.00
CH+CH2O<=>H+CH2CO	9.460E+13	.000	-515.00
CH+HCCO<=>CO+C2H2	5.000E+13	.000	.00
CH2+O2=>OH+H+CO	5.000E+12	.000	1500.00
CH2+H2<=>H+CH3	5.000E+05	2.000	7230.00
2CH2<=>H2+C2H2	1.600E+15	.000	11944.00
CH2+CH3<=>H+C2H4	4.000E+13	.000	.00
CH2+CH4<=>2CH3	2.460E+06	2.000	8270.00
CH2+CO(+M)<=>CH2CO(+M)	8.100E+11	.500	4510.00
CH2+HCCO<=>C2H3+CO	3.000E+13	.000	.00
CH2(S)+N2<=>CH2+N2	1.500E+13	.000	600.00
CH2(S)+O2<=>H+OH+CO	2.800E+13	.000	.00
CH2(S)+O2<=>CO+H2O	1.200E+13	.000	.00
CH2(S)+H2<=>CH3+H	7.000E+13	.000	.00
CH2(S)+H2O(+M)<=>CH3OH(+M)	4.820E+17	-1.160	1145.00
CH2(S)+H2O<=>CH2+H2O	3.000E+13	.000	.00

Reaction Form	Reaction Constant	Temperature Exponent	Activation Energy (cal/mole)
CH2(S)+CH3<=>H+C2H4	1.200E+13	.000	-570.00
CH2(S)+CH4<=>2CH3	1.600E+13	.000	-570.00
CH2(S)+CO<=>CH2+CO	9.000E+12	.000	.00
CH2(S)+CO2<=>CH2+CO2	7.000E+12	.000	.00
CH2(S)+CO2<=>CO+CH2O	1.400E+13	.000	.00
CH2(S)+C2H6<=>CH3+C2H5	4.000E+13	.000	-550.00
CH3+O2<=>O+CH3O	3.560E+13	.000	30480.00
CH3+O2<=>OH+CH2O	2.310E+12	.000	20315.00
CH3+H2O2<=>HO2+CH4	2.450E+04	2.470	5180.00
2CH3(+M)<=>C2H6(+M)	4.513E+16	-1.180	654.00
2CH3<=>H+C2H5	4.560E+12	.100	10600.00
CH3+HCO<=>CH4+CO	2.648E+13	.000	.00
CH3+CH2O<=>HCO+CH4	3.320E+03	2.810	5860.00
CH3+CH3OH<=>CH2OH+CH4	3.000E+07	1.500	9940.00
CH3+CH3OH<=>CH3O+CH4	1.000E+07	1.500	9940.00
CH3+C2H4<=>C2H3+CH4	2.270E+05	2.000	9200.00
CH3+C2H6<=>C2H5+CH4	6.140E+06	1.740	10450.00
HCO+H2O<=>H+CO+H2O	1.500E+18	-1.000	17000.00
HCO+M<=>H+CO+M	1.870E+17	-1.000	17000.00
HCO+O2<=>HO2+CO	13.45E+12	.000	400.00
CH2OH+O2<=>HO2+CH2O	1.800E+13	.000	900.00
CH3O+O2<=>HO2+CH2O	4.280E-13	7.600	-3530.00

Reaction Form	Reaction Constant	Temperature Exponent	Activation Energy (cal/mole)
C2H+O2<=>HCO+CO	3.333E+12	.000	-755.00
C2H+H2<=>H+C2H2	1.420E+11	0.900	1993.00
C2H3+O2<=>HCO+CH2O	4.580E+16	-1.390	1015.00
C2H4(+M)<=>H2+C2H2(+M)	8.000E+12	.440	86770.00
C2H5+O2<=>HO2+C2H4	8.400E+11	.000	3875.00
HCCO+O2<=>OH+2CO	3.200E+12	.000	854.00
2HCCO<=>2CO+C2H2	1.000E+13	.000	.00
O+CH3=¿H+H2+CO	3.370E+13	.000	.00
O+C2H4<=>H+CH2CHO	6.700E+06	1.830	220.00
O+C2H5<=>H+CH3CHO	1.096E+14	.000	.00
OH+HO2<=>O2+H2O	0.500E+16	.000	17330.00
DUPLICATE			
OH+CH3=>H2+CH2O	8.000E+09	.500	-1755.00
CH+H2(+M)<=>CH3(+M)	1.970E+12	.430	-370.00
CH2+O2=>2H+CO2	5.800E+12	.000	1500.00
CH2+O2<=>O+CH2O	2.400E+12	.000	1500.00
CH2+CH2=>2H+C2H2	2.000E+14	.000	10989.00
CH2(S)+H2O=>H2+CH2O	6.820E+10	.250	-935.00
C2H3+O2<=>O+CH2CHO	3.030E+11	.290	11.00
C2H3+O2<=>HO2+C2H2	1.337E+06	1.610	-384.00
O+CH3CHO<=>OH+CH2CHO	5.840E+12	.000	1808.00
O+CH3CHO=>OH+CH3+CO	5.840E+12	.000	1808.00

Reaction Form	Reaction Constant	Temperature Exponent	Activation Energy (cal/mole)
O2+CH3CHO=>HO2+CH3+CO	3.010E+13	.000	39150.00
H+CH3CHO<=>CH2CHO+H2	2.050E+09	1.160	2405.00
H+CH3CHO=>CH3+H2+CO	2.050E+09	1.160	2405.00
OH+CH3CHO=>CH3+H2O+CO	2.343E+10	0.730	-1113.00
HO2+CH3CHO=>CH3+H2O2+CO	3.010E+12	.000	11923.00
CH3+CH3CHO=>CH3+CH4+CO	2.720E+06	1.770	5920.00
H+CH2CO(+M)<=>CH2CHO(+M)	4.865E+11	0.422	-1755.00
O+CH2CHO=>H+CH2+CO2	1.500E+14	.000	.00
O2+CH2CHO=>OH+CO+CH2O	1.810E+10	.000	.00
O2+CH2CHO=>OH+2HCO	2.350E+10	.000	.00
H+CH2CHO<=>CH3+HCO	2.200E+13	.000	.00
H+CH2CHO<=>CH2CO+H2	1.100E+13	.000	.00
OH+CH2CHO<=>H2O+CH2CO	1.200E+13	.000	.00
OH+CH2CHO<=>HCO+CH2OH	3.010E+13	.000	.00
C2H+O=>CH(S)+CO	4.817E+12	0.000	456.73
CH(S)=>CH	1.900E+06	0.000	0.00
CH(S)+O2=>CH+O2	1.929E+12	0.750	0.00
CH(S)+H2=>CH+H2	1.866E+10	1.773	0.00
CH(S)+N2=>CH+N2	2.722E+12	0.600	0.00
CH(S)+H2O=>CH+H2O	9.232E+11	1.100	0.00
CH(S)+CH4=>CH+CH4	3.653E+10	1.773	0.00
CH(S)+CO=>CH+CO	7.794E+12	0.714	0.00

Reaction Form	Reaction Constant	Temperature Exponent	Activation Energy (cal/mole)
CH(S)+CO2=>CH+CO2	1.143E+11	1.100	0.00
CH(S)+C2H2=>CH+C2H2	3.166E+12	1.100	0.00
CH(S)+C2H6=>CH+C2H6	1.925E+11	1.773	0.00
CH(S)+O2=>O+HCO	6.170E+13	.000	0.00
CH(S)+H2=>H+CH2	1.107E+08	1.790	1670.00
CH(S)+H2O=>H+CH2O	1.713E+13	.000	-755.00
CH(S)+CH2=>H+C2H2	4.000E+13	.000	0.00
CH(S)+CH3=>H+C2H3	3.000E+13	.000	0.00
CH(S)+CH4=>H+C2H4	6.000E+13	.000	0.00
CH(S)+CO2=>HCO+CO	3.400E+12	.000	690.00
CH(S)+CH2O=>H+CH2CO	9.460E+13	.000	-515.00
CH(S)+HCCO=>CO+C2H2	5.000E+13	.000	.00
CH(S)+O2=>OH+CO	2.000E+13	0.000	0.00
O+CH(S)=>H+CO	5.700E+13	.000	.00
OH+CH(S)=>H+HCO	3.000E+13	.000	.00
HCO+O=>OH(S)+CO	2.900E+13	0.000	456.73
OH(S)=>OH	1.700E+06	0.000	0.00
OH(S)+H2=>OH+H2	9.500E+18	-0.400	0.00
OH(S)+N2=>OH+N2	5.600E+18	-0.550	0.00
OH(S)+O2=>OH+O2	5.600E+18	-0.350	0.00
OH(S)+H2O=>OH+H2O	2.700E+19	-0.350	0.00

Reaction Form	Reaction Constant	Temperature Exponent	Activation Energy (cal/mole)
OH(S)+CH4=>OH+CH4	4.900E+18	-0.200	0.00
OH(S)+CO=>OH+CO	2.400E+19	-0.470	0.00
OH(S)+CO2=>OH+CO2	5.100E+19	-0.560	0.00
OH(S)+H2=>H+H2O	2.160E+08	1.510	3430.00
OH(S)+HO2=>O2+H2O	2.900E+13	.000	-500.00
OH(S)+H2O2=>HO2+H2O	1.750E+12	.000	320.00
DUPLICATE			
OH(S)+H2O2=>HO2+H2O	5.800E+14	.000	9560.00
DUPLICATE			
OH(S)+C=>H+CO	5.000E+13	.000	0.00
OH(S)+CH=>H+HCO	3.000E+13	.000	0.00
OH(S)+CH2=>H+CH2O	2.000E+13	.000	0.00
OH(S)+CH2=>CH+H2O	1.130E+07	2.000	3000.00
OH(S)+CH2(S)=>H+CH2O	3.000E+13	.000	.00
OH(S)+CH3=>CH2+H2O	5.600E+07	1.600	5420.00
OH(S)+CH3=>CH2(S)+H2O	6.440E+17	-1.340	1417.00
OH(S)+CH4=>CH3+H2O	1.000E+08	1.600	3120.00
OH(S)+CO=>H+CO2	4.760E+07	1.228	70.00
OH(S)+HCO=>H2O+CO	5.000E+13	.000	.00
OH(S)+CH2O=>HCO+H2O	3.430E+09	1.180	-447.00
OH(S)+CH2OH=>H2O+CH2O	5.000E+12	.000	.00
OH(S)+CH3O=>H2O+CH2O	5.000E+12	.000	.00

Reaction Form	Reaction Constant	Temperature Exponent	Activation Energy (cal/mole)
OH(S)+CH3OH=>CH2OH+H2O	1.440E+06	2.000	-840.00
OH(S)+CH3OH=>CH3O+H2O	6.300E+06	2.000	1500.00
OH(S)+C2H=>H+HCCO	2.000E+13	.000	.00
OH(S)+C2H2=>H+CH2CO	2.180E-04	4.500	1000.00
OH(S)+C2H2=>H+HCCOH	5.040E+05	2.300	13500.00
OH(S)+C2H2=>C2H+H2O	6.000E+12	0.000	7000.00
OH(S)+C2H2=>CH3+CO	4.830E-04	4.000	-2000.00
OH(S)+C2H3=>H2O+C2H2	5.000E+12	.000	.00
OH(S)+C2H4=>C2H3+H2O	3.600E+06	2.000	2500.00
OH(S)+C2H6=>C2H5+H2O	3.540E+06	2.120	870.00
OH(S)+CH2CO=>HCCO+H2O	7.500E+12	.000	2000.00

Appendix B

PREMIX Modifications

B.1 Program structure modifications

The single major modification of the program structure is the ability to move from one solution to another desired solution in small increments, where the solution of the increments is not written into the solution file. In the published version of the PREMIX flame code, the continuation problem constitutes the only way to make one solution the initial guess for another solution. The continuation problem functionality is retained in the modified version of PREMIX. Added to the program is the ability to choose whether or not the solution of the continuation problem is written into the solution file. Sometimes a continuation problem constitutes an intermediate step between desired conditions and would take up needless space in the solution file in the old version of the program. The new keyword "EXCE" has been added and is described below in Section B.2.

Numerical stability and speed of calculation is greatly enhanced if in moving from one condition to another, small increments of change are used. In order to avoid writing very long input problem files, another feature has been added to PREMIX. Using two keywords, "INCR" and "IGOL", which are described below in Section B.2, it is possible to have the program vary the flow–rate, equivalence ratio or grid refinement parameters in small increments until a goal value is attained. In the process, the increments are increased from their initial value if the initial parameter change was successful and decreased if no solution was able to be found for the initial parameter change. The increment has a fixed maximum and a fixed minimum. If the fixed minimum increment is reached, the program exits with an error message.

The remainder of the program structure was left intact with all other changes stemming from the addition of unknowns in the problem and a change in the governing equations, depending on the type of problem to be solved. In its present version, PREMIX has all of the capabilities of the original program. However, the output file contains the honeycomb solid temperature no matter what the problem solved because the number of unknowns is still fixed and does not vary with the problem considered. In the case of non-honeycomb combustion problems, a dummy equation

for the honeycomb temperature is solved. The computational penalty for the addition of a dummy equation appears to be very small based on the PREMIX burner stabilized flame calculations performed for the Bunsen type burner model. (See Section 7.3.3)

The modified version of PREMIX also allows the user to specify the maximum number of data points, rather than having a set number above which the computational domain cannot be refined. In the old version of PREMIX the number of points was artificially limited to 69 points. The modified version of PREMIX also generates another file for more compact post–processing. The file contains one line of summary data for each case that was printed to the output file. The filename for the summary output file is determined using a filename dialog at the start of the program. The program will ask for the EXCEL output filename. The post–processing performed is programmed in "Postprocess.f" and for the purposes of the present work included the integration of the chemiluminescence species profiles of OH^* as well as CH^*. The program also identified important temperatures and logged the equivalence ratio, flow–rate, inlet temperature and inlet temperature gradient for the current calculation. For a large number of cases, post–processing should be performed in "Postprocess.f" to achieve a large time savings. Post-processing of the written output file has also been made easier by modifying the output data–file format. The output data–file no longer is limited to 80 columns of text but stretches on as far as required by the number of unknowns, greatly decreasing the difficulty in post–processing using spreadsheet programs.

B.2 Description of added keywords

The following subsections will describe each of the available keywords previously not recognized by PREMIX.

B.2.1 HOCO - the honeycomb burner problem

The HOCO keyword is called to signal that the flame problem is to be solved considering the honeycomb burner governing equations as described in Chapter 8. The

keyword should not be called before another burner stabilized flame problem is solved. Calling the HOCO keyword causes the program to initialize the solid honeycomb part of the computational domain located to the left of the axial coordinate zero location. Accordingly, XSTRT for the previous burner stabilized flame problem should be set to 0 cm.

B.2.2 RADF - radiation and other heat–loss

The RADF keyword specifies that a modified energy equation, including heat–loss should be solved. The radiative heat–loss model is specified in the routines "radinteg.f" and "radprop.f". The convective heat–loss model is specified in the routine "convection.f". The RADF keyword considers only heat–losses if the problem considered is not a honeycomb burner modeling problem. For the honeycomb burner problem, calling RADF also enables the heat–transfer coupling between the solid honeycomb and the gases. It is not recommended to run a honeycomb burner modeling problem without first having specified radiation heat–loss using the RADF keyword.

B.2.3 INCR and IGOL - small step parameter variation

The keywords INCR and IGOL are always called together. The first keyword specifies the variable to be incrementally changed. The second keyword specifies the target value for the parameter. INCR followed by the number 1 specifies that an equivalence ratio variation is to be undertaken. INCR followed by the number 2 specifies that a flow–rate variation is desired. INCR followed by the number 3 specifies that a parallel curvature and gradient refinement variation is desired.

The value added after the keyword IGOL specifies the target value of the parameter or parameters to be varied. It is important to note that the equivalence ratio calculation is based on the combustion of methane. The units for flow–rate are g/(sec-cm^2) for all calculations except honeycomb burner calculations where the units become g/sec. For an INCR value of 3, the curvature and gradient parameters are set equal and varied together until both reach the target value specified by IGOL.

B.2.4 EXCE - writing output

The EXCE keyword causes the program to write the output of the current modeling calculation to the two text output files. The keyword allows large parameter variations without undue writing in the output files. Using the keyword allows output files to be formed which exclusively contain desired model output. The EXCE keyword does not disable writing program progress flags and care should be taken in the correct specification of the PRNT keyword to avoid unnecessary text output.

B.2.5 Programming new keywords

The addition of keywords to the capabilities of PREMIX is not difficult and no advanced user should shy away from attempting to add some other desired keyword to the list of accepted keywords. The structure of the program is transparent enough that the addition of new keywords does not represent a major programming challenge. The routine in which keyword definitions are handled is named "RDKEY" and is located inside "premix.f". The routine is only called by one routine called "FLDRIV", which is the major center program node for PREMIX operation.

Appendix C

Optical System Design

C.1 Geometrical Optics

The lens system design used in the premixed flame study is based entirely on geometrical optics using the thin lens assumption. Any errors incurred in assuming that the lenses are thin are corrected for by the experimental procedure described in Section 3.3. The present development allows a preliminary starting point to be obtained for the global chemiluminescence measurement system and shows how local chemiluminescence measurements are to be made.

The equation that forms the basis of all thin–lens calculations is the Gaussian lens formula given in Equation C.1.(Hecht, 1987) The formula relates the object location and image location through the focal length for a symmetrical bi–convex lens.

$$\frac{1}{f} = \frac{1}{s_o} + \frac{1}{s_i} \tag{C.1}$$

The ray–tracing process is a geometrical application of the Gaussian lens formula. The Gaussian lens equation allows the following elementary ray–tracing laws to be formulated: Rays through the center of the lens do not bend; rays through the focal point ahead of the lens become parallel after the lens and rays parallel to the optical path ahead of the lens pass through the focal point after the lens. The ray tracing principles allow geometrical laws to be used to completely calculate all aspects of the image based on the object characteristics. The ray tracing technique is illustrated in Figure C.1 for a single lens. The ray–tracing technique thus for example gives the ratio of the image height to the object height as the ratio of the image distance to the object distance using similar triangles.(Hecht, 1987)

C.2 The Two Lens System

The resulting image of a two–lens system is the combination of two single lenses where the object of the second lens is the image of the first lens. If the image lies beyond the second lens, then the object distance is negative, but this does not alter the validity of the Gaussian lens equation.

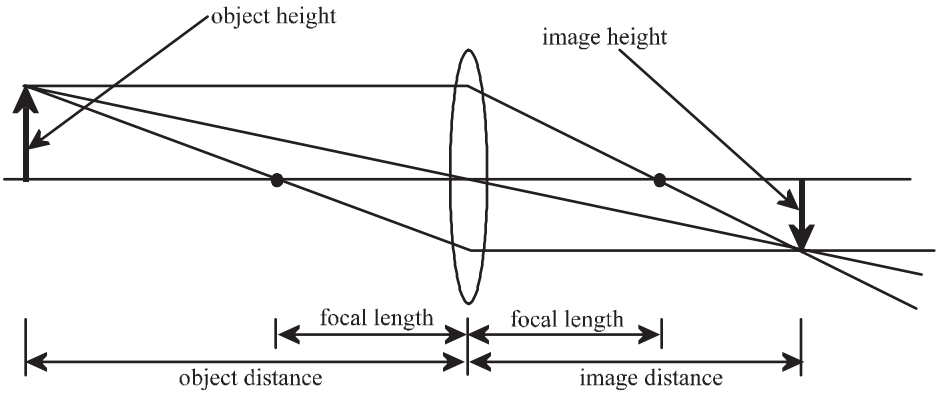

Figure C.1: Schematic of ray–tracing technique

The process of applying ray–tracing to the two-lens system is illustrated in Figure C.2. The second image is constructed from two rays. The first ray is easily identified to be the ray that passes through the first lens focal point becomes parallel and then after the second lens, passes through its focal point. The second ray is found by using the first image as a guide. The ray that passes through the center of the second lens while forming the first–lens image remains unaltered with the addition of the second lens. The final image location of the two–lens system is thus given by the intersection of these two rays. The third ray indicated to construct the final image is a ray of special importance to the light collection apparatus mounted to the right of the second lens.

The angle indicated as the critical angle is the angle of the steepest participating ray in the formation of the final image. The ray is important in light collection because of the limited numerical aperature of the fiber optic termination. Numerical aperature is calculated by taking the sine of the interior angle of the acceptance cone of the light collection device in question. A large critical angle requires a large numerical

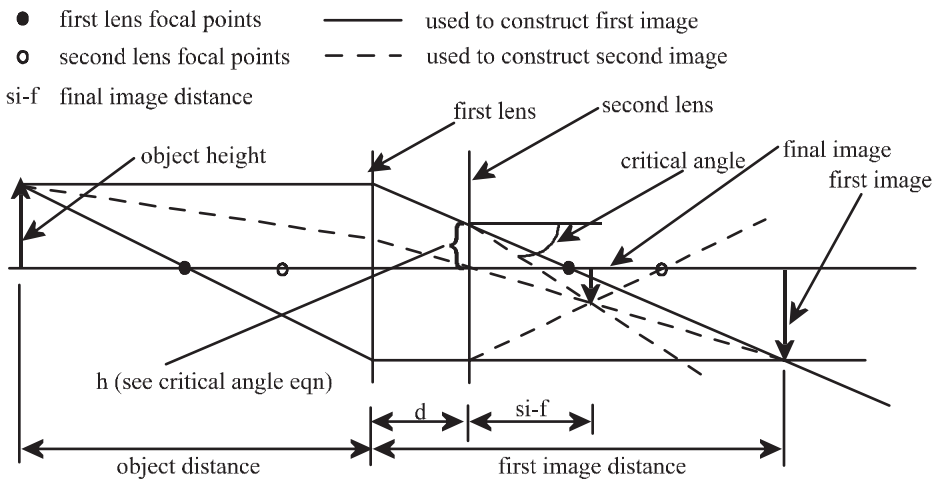

Figure C.2: The two–lens type optical system

aperature. The small diameter fiber optic cable termination only has a numerical aperature of 0.2, corresponding to a cone–angle of 11.5 degrees. The large diameter fiber optic cable termination has a numerical aperature of 0.48, corresponding to a cone–angle of 28.7 degrees. The critical angle is calculated using the expression given in Equation C.2.

$$\tan\theta_{crit} = \frac{h - \frac{s_{i-1}}{s_{o-1}}\frac{s_{i-2}}{s_{o-2}}\frac{D_1}{2}}{s_{i-2}} \qquad \text{(C.2)}$$

where:

$$h = \frac{D_1}{2} - \frac{d\ D_1}{2\ f_1}$$

C.3 Light Collection

The calculations detailed to this point identify the location of the image behind the second lens and some of its characteristics such as the critical angle. The receiving optical device has not yet entered the calculation. The calculations described in

the present section deal with calculating how much of the emitted light actually is collected by the fiber optic cable.

To determine the percentage of total emitted light collected by the first lens, the object and lens will be assumed to be infinitely wide (dimension perpendicular to page has no bound). The assumption allows the optics to be analyzed in plane view, greatly simplifying the mathematics involved in the calculation. The error incurred in making the assumption may be significant, but since the results will only be used relative to one another, the conclusions drawn remain valid. The fraction of light collected by the first lens from a point source is the ratio of the interior angle of the accepted rays divided by the total angle of radiation which for the plane case is equal to $2\,\pi$. The point source represents a differential element of the total radiation source. To obtain the total fraction of light collected by the first lens, the local fraction must be integrated over the entire emitting object. The process is illustrated on the left side of Figure C.3. The collection of expressions allowing the integration is given in Equation C.3. Note that the fraction of light collected is not necessarily equal to all the rays hitting the lens, due to the limitation by the lens' numerical aperature (NA).

$$\begin{aligned} F_{in} &= \frac{4}{L}\int_0^{\frac{L}{2}} \frac{\theta_H - \theta_L}{2\,\pi}\,dl \\ \theta_H &= min\left(\frac{\pi}{2} + \arctan\frac{\frac{H_o}{2} - l}{d}\;,\;\frac{\pi}{2} + \arctan NA_{lens}\right) \\ \theta_L &= min\left(\arctan\frac{d}{\frac{H_o}{2} + l}\;,\;\arctan NA_{lens}\right) \end{aligned} \tag{C.3}$$

The calculation to find how much light actually is collected by the fiber optic cable termination is similar to the above but complicated by the fact that the source is in this case no longer diffuse. The source in the calculation is the second lens. The rays passing through the lens all will pass through the image generated to the right of the second lens. The fiber optic cable termination is located in the image plane. The setup is illustrated on the right side of Figure C.3. The percentage of the light forming the image actually collected by the fiber optic cable is calculated again as a ratio of angles. The angles are shown in Figure C.3. The rays are limited

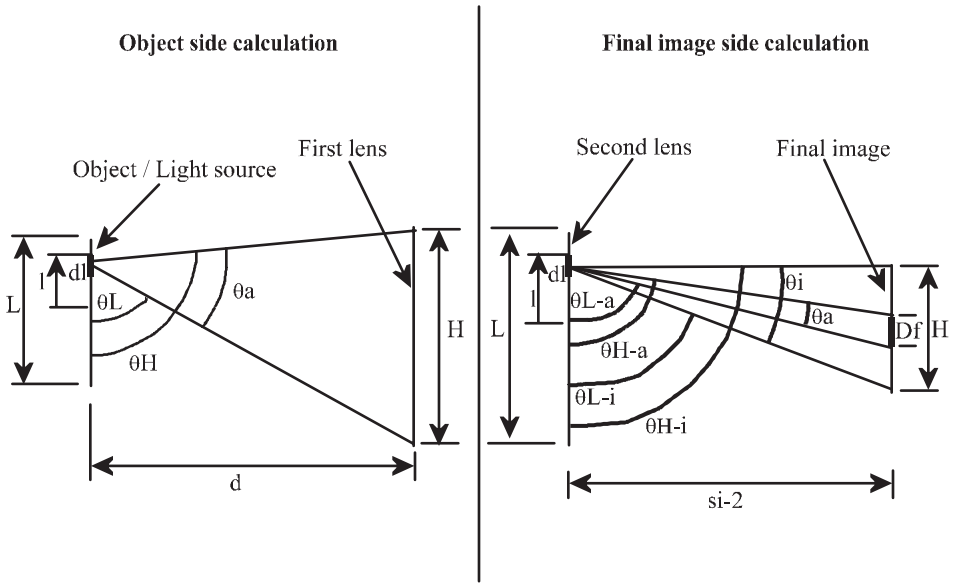

Figure C.3: Illustration of calculations involving the percentage of light collected

to the critical angle calculated above in Section C.2. The set of expressions allowing integration of the percentage of light collected by the fiber optic cable termination is given in Equation C.4. Referring back to Figure C.3 may help in the interpretation of the quantities used in the expressions. The percentage of light collected by the fiber optic cable that was emitted by the original radiation source can be calculated by multiplying the two fractions calculated in Equation C.3 and Equation C.4.

$$
\begin{aligned}
F_{fin} &= \frac{4}{L}\int_0^{\frac{L}{2}} \frac{\theta_a}{\theta_i}\, dl \\
\theta_a &= \theta_{H-a} - \theta_{L-a} \\
\theta_{H-a} &= min\left(\frac{\pi}{2} + \arctan\frac{\frac{H}{2} - f_2 - l}{s_{i-2}}\ ,\ \arctan NA_{fiber} + \frac{\pi}{2}\right) \\
\theta_{L-a} &= min\left(\arctan\frac{s_{i-2}}{\frac{H}{2} - f_2 + l}\ ,\ \arctan NA_{fiber}\right) \\
\theta_i &= \theta_{H-i} - \theta_{L-i} \\
\theta_{H-i} &= min\left(\ \frac{\pi}{2} + \arctan\frac{\frac{H}{2} - l}{s_{i-2}}\ ,\ \theta_{crit} + \frac{\pi}{2}\right) \\
\theta_{L-i} &= min\left(\ \arctan\frac{s_{i-2}}{\frac{H}{2} + l}\ ,\ \theta_{crit}\right)
\end{aligned}
\tag{C.4}
$$

The actual calculations of the above integrals and resulting numbers, were performed using a trapezoidal rule integration scheme with 500 evenly spaced increments. Increasing the number of elements to 1000 did not influence the results significantly.

The calculations above are not only limited to plane optics but also to zero–depth objects. Depth is measured by how much the object to lens distance varies over the entire radiation source. A common assumption is that if the depth is much smaller than the average object to lens distance then effects of depth on the optics may be ignored. The requirement for a large object to lens distance relative to object depth is met for both global and local experimental setups on the Bunsen type burner as well as the global chemiluminescence experimental setup used on the honeycomb burner.

The calculations above are not useful in their absolute measure of the percentage of light collected. However, a series of calculations of the type described above can yield very important relative intensity collection data. For example, calculations clearly show the large advantage of using the two–lens optical system in comparison to a bare fiber. The most important contribution from the calculations however is the ability to calculate the dot size of the experimental setup. The dot size is the maximum diameter of the object which is uniformly imaged onto the fiber optic cable termination. The following paragraph describes dot–size calculations.

The basis of the calculation is the percentage of light collected calculation for

an object exactly the same size as the optical fiber. All of the light from this size object that hits the first lens within its numerical aperature will be collected by the optical fiber. As the object height is increased from the base height, less and less of the incremental light increase will be collected. The percentage of light collected from an incrementally larger object is compared back to the percentage of light collected from the base object size. Using the two percentages, it is possible to calculate what fraction of light from the incremental object area is collected relative to how much was collected from the base object size. The calculation is shown explicitly in Equation C.5. The calculation uses the circular areas of the emitting objects as weighting factors. As the object size is increased, a point will be reached where the image size becomes bigger than the optical fiber, and the fraction of light collected from the incremental area will be decreasing rapidly. A plot of the fraction of light collected from the incremental area was shown in Figure 2.7 and is reproduced here in Figure C.4.

$$F_{incr} = \frac{F_{tot}\ A_{tot}\ -\ F_{old}\ A_{old}}{A_{incr}} \tag{C.5}$$

For the global chemiluminescence experimental setup on the Bunsen type burner, the dot size was designed to be 12 mm, covering more than the exit diameter of the burner to account for the flame–base being larger than the burner exit diameter. For local chemiluminescence measurements, the dot size was reduced to 0.5 mm to get relatively good spatial resolution across the Bunsen type flame. For the honeycomb burner setup, the large diameter fiber was used along with a dot size equal to the burner exit diameter, since the flame is confined to this area.

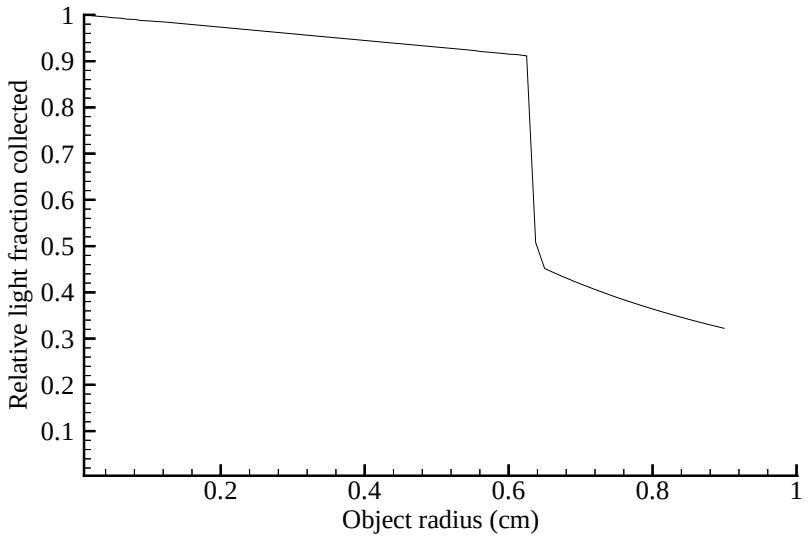

Figure C.4: Relative fraction of light collected from incremental area

Bibliography

Bandaru, R., Miller, S., Jong, L., and Santavicca, D. A. (1999). Sensors for measuring primary zone equivalence ratio in gas turbine combustors. *Proceedings of SPIE*, 3535:104–114.

Becker, K., Kley, D., and Norstrom, R. (1977). OH^* chemiluminescence in hydrocarbon atom flames. *Fourteenth Symposium (International) on Combustion*, pages 405–411.

Beyler, C. and Gouldin, F. (1981). Flame structure in a swirl stabilized combustor inferred by radiant emission measurements. *Eighteenth Symposium (International) on Combustion*, pages 1011–1019.

Bloxsidge, G., Dowling, A., Hooper, N., and Langhorne, P. (1988a). Active control of reheat buzz. *AIAA Journal*, 26(7):783–790.

Bloxsidge, G., Dowling, A., and Langhorne, P. (1988b). Reheat buzz: An acoustically coupled combustion instability. part 2. theory. *Journal of Fluid Mechanics*, 193:445–473.

Cho, S., Kim, J., and Lee, S. (1998). Characteristics of thermoacoustic oscillation in a ducted flame burner. *Proceedings of the 36th Aerospace Sciences Meeting & Exhibit AIAA 98-0473*.

Chomiak, J. (1972). Application of chemiluminescence measurement to the study of turbulent flame structure. *Combustion and Flame*, 18:429–433.

Clark, T. (1958). Studies of OH, CO, CH and C_2 radiation from laminar and turbulent propane-air and ethylene-air flames. *NACA Technical Note 4266*.

Dandy, D. and Vosen, S. (1992). Numerical and experimental studies of hydroxyl radical chemiluminescence in methane-air flames. *Combustion Science and Technology*, 82:131–150.

Davidson, D., Dean, A., DiRosa, M., and Hanson, R. (1991). Shock tube measurements of the reactions of CN with o and o2. *International Journal of Chemical Kinetics*, 23(11):1035–1050.

Devriendt, K. and Peeters, J. (1997). Direct identification of the CH^* chemiluminescence in C_2H_2 / O / H atomic flames. *Journal of Physical Chemistry A*, 101:2546–2551.

Engstrom, R. (1980). *Photomultiplier Handbook*. RCA, Lancaster Pa.

Fluent Inc. (1998). *Fluent 5.0 User's Guide*. Fluent Inc., Lebanon NH 03766.

Frenklach, M., Wang, H., and Rabinowitz, J. (1992). Optimization and analysis of large chemical kinetic mechanisms using the solution mapping method - combustion of methane. *Progress in Energy Combustion Science*, 18:47–73.

Garland, N. and Crosley, D. (1986). On the collisional quenching of electronically excited OH, NH and CH in flames. *Twenty-first Symposium (International) on Combustion*, pages 1693–1702.

Gaydon, A. (1974). *Spectroscopy of Flames*. Chapman and Hall, London, 2nd edition.

Gaydon, A. and Wolfhard, H. (1979). *Flames*. Chapman and Hall, London.

Glass, G., Kistiakowsky, G., Michael, J., and Niki, H. (1965). NEED. *Tenth Symposium (International) on Combustion*, pages 513–525.

Hastings Instruments (1994). *Hastings Model HFM Mass Flow–Meters*. Teledyne Brown Engineering - Hastings Instruments, P.O. BOX 1436 Hampton VA 23661 USA.

Hecht, E. (1987). *Optics*. Addison-Wesley, Reading Ma.

Hottel, H. and Sarofim, A. (1967). *Radiative Heat –Transfer NEED Publisher*, chapter 2, page 55. McGraw-Hill.

Hurle, I., Price, R., Sugden, T., and Thomas, A. (1968). Sound emission from open turbulent premixed flames. *Proceedings of the Royal Society Series A*, 303:409–427.

Ikeda, Y., Kojima, J., and Nakajima, T. (2000). Local damköhler number measurement in turbulent Methane/Air premixed flames by local OH*, CH* and c_2* chemiluminescence. *AIAA paper 2000-3395*.

Jarrel-Ash (1971). *Jarrel-Ash Model 82-000 Series 0.5 M Ebert Scanning Spectrophotometer*. Jarrel-Ash division of Thermo Vision Colorado (TVC), Waltham MA 02154.

Joklik, R., Daily, J., and Pitz, W. (1986). Measurements of CH radical concentrations in an Acetylene/Oxygen flame and comparisons to modeling calculations. *Twenty-first Symposium (International) on Combustion*, pages 895–904.

Ju, Y., Guo, H., Liu, F., and Maruta, K. (1999). Effects of the lewis number and radiative heat loss on the bifurcation and extinction of CH4/O2-n2-he flames. *Journal of Fluid Mechanics*, 379:165–190.

Kee, R., Grcar, J., Smooke, M., and Miller, J. (1993). A fortran program for modeling steady laminar one-dimensional premixed flames. Technical Report SAND85-8240 UC-401, Sandia National Laboratories.

Khanna, V., Vandsburger, U., Saunders, W., Bauman, W., and Hendricks, A. (2000). Dynamic analysis of burner stabilized flames part i: Laminar premixed flame. In *American Flame Research Committee (AFRC) International Symposium, Newport Beach, CA, USA, September 2000*.

Kojima, J., Ikeda, Y., and Nakajima, T. (2000). Detail distributions of OH*, CH* and c_2* chemiluminescence in the reaction zone of laminar premix Methane/Air flames. *AIAA paper 2000-3394*.

Kreith, F. and Bohn, M. (1993). *Principles of Heat Transfer*. West Publishing.

Krishnamahari, S. and Broida, H. (1961). Effect of molecular oxygen on the emission spectra of atomic oxygen-acetylene flames. *Journal of Chemical Physics*, 34(5):1709–11.

Langhorne, P. (1988). Reheat buzz: An acoustically coupled combustion instability. part 1. experiment. *Journal of Fluid Mechanics*, 193:417–443.

Marchese, A., Dryer, F., Nayagam, V., and Colantonio, R. (1996). Hydroxyl radical chemiluminescence imaging and the structure of microgravity droplet flames. *Twenty-sixth Symposium (International) on Combustion*, pages 1219–1226.

Najm, H., Paul, P., Mueller, C., and Wyckoff, P. (1998). On the adequacy of certain experimental observables as measurements of flame burning rate. *Combustion and Flame*, 113:312–332.

National Instruments (1996). *LabVIEW User Manual Part No. 320999 A-01*. National Instruments.

Paschereit, C., Gutmark, E., and Weisenstein, W. (1998). Excitation of thermoacoustic instabilities by the interaction of acoustics and unstable swirling flow. *AIAA Journal*, 45(4):108–117.

Paschereit, C. O. and Polifke, W. (1998). Investigation of the thermoacoustic characteristics of a lean premixed gas turbine burner. *Proceedings of the IGTI 98-GT-582*.

Poinsot, T., Echekki, T., and Mungal, M. (1992). A study of the laminar flame tip and implications for premixed turbulent combustion. *Combustion Science and Technology*, 81:45–73.

Price, R., Hurle, I., and Sugden, T. (1968). Optical studies of the generation of noise in turbulent flames. *Twelfth Symposium (International) on Combustion*, pages 1093–1102.

Renlund, A., Shokoohi, F., Reisler, H., and Wittig, C. (1981). NEED title. *Chemical Physics Letters*, 84(2):293.

Richards, G. A. and Janus, M. (1998). Characterization of oscillations during premix gas turbine combustion. *Journal of Engineering for Gas Turbines & Power-Transactions of the ASME*, 120(2):294–302.

Samaniego, J., Egolfopoulos, F., and Bowman, C. (1995). CO_2^* chemiluminescence in premixed flames. *Combustion Science and Technology*, 109:183–203.

Schefer, R. (1997). Flame sheet imaging using CH chemiluminescence. *Combustion Science and Technology*, 126:255–270.

Smith, P., Golden, D., Frenklach, M., Moriarty, N., Eiteneer, B., Goldenberg, M., Bowman, C., Hanson, R., Song, S., Gardiner, W., Lissianski, V., and Qin, Z. (1999). *http:// www.me.berkeley.edu/gri_mech/*.

Smooke, M., editor (1991). *Reduced Kinetic Mechanisms and Asymptotic Approximations for Methane-Air Flames*, volume 384. Springer-Verlag Lecture Notes in Physics.

Sun, C., Sung, C., and Law, C. (1994). On adiabatic stabilization and geometry of bunsen flames. *Twenty-fifth Symposium (International) on Combustion*, pages 1391–1398.

Turns, S. (1998). *An Introduction to Combustion*. McGraw-Hill, 2nd edition.

Vita

The author was born in Stuttgart Germany on June 23, 1974. At the age of three, he moved to the tiny country of Luxembourg where he stayed for the next 13 years. In 1990, he moved to Princeton, Massachusetts. He graduated from Wachusett Regional High School in 1993 and moved on to pursue a Bachelor's degree in Engineering at Virginia Tech. After beginning studies in aerospace engineering, the internship experience at MPR Associates of Alexandria, Virginia led to a change in engineering disciplines. He completed the Bachelor's degree in the department of mechanical engineering in May 1998, graduating Summa Cum Laude. He was awarded an NSF graduate fellowship to pursue a doctoral degree. Continuing a rewarding undergraduate research experience, he chose to work under Dr. Uri Vandsburger to pursue a doctoral degree in mechanical engineering, with the help of an NSF graduate fellowship. Along the way, the separate research interests of chemiluminescence and fluid mechanics allowed for an intermediate stepping stone, represented by the master's degree. In the fall of 2000, he became a United States citizen. Upon the completion of the master's degree, the doctoral degree will be pursued full–time in the area of swirling flow stability.

Permanent Address: 5660 Prices Fork Rd.
Radford VA 24141
USA